Monte-Carlo Study of Precision Magnetic Spectrometer With Planar Geometry.

A.A. Khrutchinsky Yu.Yu. Lachin [1] V.I.Selivanov

[a] *General and Nuclear Physics Institute, Russian Research Centre "Kurchatov Institute", Moscow 123182, Russia*

Abstract

The possibility of reconstructing the true mean initial energy at the origin employing a detector having a linear dependence of mean energy losses on path length in its components is demonstrated. A Monte-Carlo study of a magnetic spectrometer with planar drift chambers orthogonal to the magnetic field direction has been done. Simulations were carried out for positrons in the range $20 \div 50$ MeV in a magnetic field $B = 2$ T and DME as the drift gas. It is shown that 2 keV reconstruction accuracy of a mean energy at the origin can be achieved without using any specific information about the value of energy loss of positrons in the detector. A suggested "sliding" technique provides track reconstruction with a reliable confidence level by eliminating most large kinks. Application of $1/\cos\theta$ energy loss dependence to continuous spectrum reconstruction is studied. The influence of the Lorentz drift angle and positive ion effects on reconstruction accuracy has been analyzed. It is shown that though under certain circumstances the Lorentz drift effect can cause significant shifts of a mean reconstructed energy and distortions of the continuous spectrum, these distortions become negligible for a distributed source or one averaged over 2π azimuthal angle range and a continuous flat spectrum can be reconstructed with total statistics up to 10^{12} in 4π solid angle without systematic error.

Key words: Spectrometer, Drift Chamber, Lorentz angle.

1 Introduction

One of the common tasks in many experimental setups is the reconstruction of the original energy of particles coming to a detector from the target through

[1] Corresponding author. Phone: 7-(095)196-7058 Fax: 7-(095)882-5804 E-mail: yuyu@triumf.ca

some amount of matter. The usual way to correct the energy measured in detector is the use of GEANT or EGS4 simulation. This approach depends on the accuracy of the tracking packages and requires the knowledge of the energy losses and the exact amount of matter prior to detector. At the same time, the mean energy loss of particles is proportional to path length in matter and this can be utilized (with the proper detector design) to find the mean original energy without the actual knowledge of the energy losses value.

The applicability of this approach depends on the design of a detector. We consider below as an example a proposed magnetic spectrometer with drift chambers. Its main distinguishing feature is the possibility to reconstruct the mean energy of detected particles at the level of accuracy of a few keV and to reconstruct a continuous spectra without distortions. The need for such a detector design arises from TRIUMF Experiment 614. The goal of E614 is the measurement of the Michel parameters in $\mu \to e$ decay at a level of precision of a few 10^{-4}. The proposed spectrometer has $\approx 1.5\pi$ solid angle acceptance. Such a detector can be used, in principle, for experiments in particle physics requiring high precision reconstruction of a continuous spectrum or the mean energy of narrow peak.

The advantage of the proposed spectrometer is defined, first of all, by its planar geometry. A planar target and the assembly of planar drift chambers (PDC) is arranged perpendicular to the magnetic field (Fig.1). In such a layout the mean energy loss of particles in the detector is given by $\Delta E(E, \theta) = \Delta E(E, \theta = 0)/\cos\theta$, where θ is the polar angle with respect to magnetic field, E is the particle energy. This formula simply expresses the fact that the effective degrader thickness (path length) grows with the θ. The $1/\cos\theta$ dependence is obvious for the planar target, for a gas gap and for the planar cathode plane. It also applies to wires even though the energy loss does not have this simple dependence on θ (for cylindrical wires) since the probability of hitting a wire does have a $1/cos\theta$ dependence on θ. This $1/\cos\theta$ dependence is valid only on average and is violated by scattering and radiative interactions with the detector matter. The level of this violation is estimated in section 4.2.

The details of the detector are presented in section 2.

In sections 3, 4.1 a "sliding" technique of track reconstruction is suggested to select and fit of a particle track segment inside the detector which is most free of substantial kinks due to large energy loss and/or scattering events.

The influence of the Lorentz drift angle and positive ion effects on reconstruction accuracy are estimated in sections 4.3, 4.4.

2 Description of detector.

Our Monte-Carlo study was carried out for the proposed detector design a schematic view of which is presented on Fig.1 together with sample positron helices in a $B = 2.35$ T field at energies 30 and 53 MeV and polar angles $\theta_0 = 5°, 10°, 60°, 88°$.

Detector specification downstream (Fig.1):

- The stopping target is a thin 20 mg/cm^2 foil. It also serves as a high voltage plane for proportional chambers PC(-1X) and PC(+1X) (Fig.2). Simulations were made for Al and Be targets.
- Identical (X+Y) PCs on both sides of the stopped target are indicators of muon stops inside the target. These PCs serve as the zero time master with 2.5 ns(RMS) time resolution for the outgoing positron registration. A "fast" drift gas $CF_4/ISO(80/20)$ is used. PCs performance with this gas was investigated in [1].
- 20 mm helium gap between (X+Y) PCs and the PDC pair closest to the target is introduced for better separation of an ingoing muon from outgoing upstream small polar angle positrons.
- Eight pairs ($\pm1, \ldots, \pm8$) of (X+Y) PDC planes measure positron helices. They are interleaved by 40 mm helium gaps introduced to improve detector resolution at small angles. "Slow" and "cold" drift gas, DME (C_2H_6O) is used in all PDCs.

Upstream and downstream parts of the detector are identical.

In what follows, all calculations were made for one specific example of detector whose PC and PDC specifications are presented in Table 1.

3 Simulation technique.

In further analysis we shall consider only one half of the detector (downstream of the stopping target) and split it logically into two parts. The first part consists of the stopped target, two proportional chambers PC(+1X), PC(+1Y), a 20 mm helium gap and the H.V. plane of the first drift chamber PDC(+1X) (See Fig.2). Positron helix is not tracked in this area. The second part begins from PDC(+1X) gas volume. Measurements in these chambers are used in helix tracking.

The EGS4 code system was used for Monte Carlo simulation of positron transport in the magnetic field of the detector. EGS4 code takes into account all interaction of particles with materials at every step. Essential components of the code are the subroutines:

- Geometry set-up for given parameters of the proportional and drift chambers and helium gaps.
- Calculation of intersection point of particle track with region boundaries.
- Tracking of charged particles in the magnetic field using Bunieman algorithm [2]. Step size of integration was defined by track curvature, distance from particle to a nearest region boundary and minimal size step for correct description of multiple scattering of particles in EGS4.
- Calculation of minimal distance from a track to sense wires of drift cells the track passed through, these distances were later used for as input for track reconstruction code.

We have chosen a simple global fit of e^+ helix, although it is clear that in the presence of strong scattering of the positron by detector materials the Kalman filter technique [3] can be more suitable. A new technique is suggested as an intermediate step to the Kalman filtering. We named it "sliding". The positron is tracked by EGS4 through the full detector. The helix is then fitted sequentially using subsets of four (X+Y) PDC pairs (Fig.1) *1234,2345, 3456, 4567*, and *5678*. We shall call each such four pair subset a *slide*. The fit result will be retained (selected) for a slide with the maximal confidence level value (χ^2 is not used for the selection because the number of wire hits in slides varies from slide to slide). Thus, the total statistics will be distributed between the slides. In EGS4 simulation positron source was uniformly distributed over a 20 mm diameter cylindrical volume within the 20 mg/cm^2 stopping target. The initial azimuthal angle distribution was uniform in the interval $[0, 2\pi]$.

We have simulated with EGS4 helices for several initial energies E_0 and angles θ_0 which were then reconstructed. The multiple scattering σ_{MS} were found from the EGS4 simulation. The EGS4 simulated shortest distance from a track to a sense wire was then randomized according to the PDC space resolution σ_{PDC}. The helix was fit to a model given by the equations:

$$
\begin{aligned}
x &= X_a + R_0(1-\lambda z)\cos(k_0 z(1+\lambda(z/2)+\phi_0) \\
y &= Y_a - R_0(1-\lambda z)\sin(k_0 z(1+\lambda z/2)+\phi_0)
\end{aligned}
\qquad (1)
$$

to minimize $\chi^2 = \sum_{i=1}^{N_{hits}} \frac{(d-d_i)^2}{\sigma_i^2}$, where $\sigma_i^2 = \sigma_{PDC}^2 + \sigma_{i,MS}^2$.

Parameters $(R_0, k_0, \phi_0, X_a, Y_a)$ representing helix parameters at the entrance to a slide ($z = 0$) were varied in the fit. The parameter $\lambda = \overline{\Delta p/p}/\Delta z$ represents an average relative momentum loss per the slide length Δz. All reconstructed parameter distributions were fitted by either the Gaussian or the generalized Breit-Wigner distribution:

$$G(x) = \alpha \left\{ 1 + [2^{1/\beta} - 1] \left(\frac{x - \overline{x}}{\gamma} \right)^2 \right\}^{-\beta} . \tag{2}$$

This Breit-Wigner function (2) fit to energy and angle distributions results in a good χ^2 value as opposed to the Gaussian fit as shown in Fig.3. Both functions produce nearly the same values of all fitted parameters except for the χ^2 value. Both functions were used in the further analysis. Either the $\gamma = FWHM/2 = HWHM$ value or the Gaussian $\sigma = \gamma(2ln2)^{-1/2} = 0.85\gamma$ was used as an error.

4 Results.

4.1 Mono-energetic peaks reconstruction.

The sliding technique is aimed at the fitting and selection of the positron track segment that is most free of substantial kinks due to large energy loss and/or scattering events. Fig.4 presents the confidence level distribution of the *"raw"* (track segment fit over the first slide region with no selection), *"slides"* (best fit of the 5 slides is retained) and "vacuum" case (fit through vacuum helix hits smeared with finite PDC resolution 50 μm, multiple scattering and energy losses turned off). One can see that the sliding technique completely removed events with $CL \approx 0$, which constitute about 20% of events in *"raw"* case. Also, sliding technique gives a more reliable track parameters estimate ($\langle CL \rangle > 0.5$).

Fig.5 illustrates the sliding technique for reconstruction of helices with initial E_0 =50 MeV and $\cos\theta_0 = 0.735$ at the origin in the stopped target. As one can see from Fig.5a there are many events with large energy losses prior to entering the $1st$ slide. Fig.5b shows that the reconstruction program successfully fits these events and returns E_{fit} close to E_{EGS}, but other events with large $E_{egs} - E_{fit}$ appear in this *"raw"* spectrum. They are events with large energy loss inside the $1st$ slide *1234*. Most of these events are not present in Fig.5c — after the slide selection technique is applied. Note also, that the mean value of $\overline{E_{fit} - E_{egs}}$=8.9 keV compared to 22 keV for the *"raw"* spectrum. Here E_{fit} and E_{egs} stand for the fitted and "true" (from EGS4 simulation) energies at the entrance to corresponding slide at the point of the closest approach of track to the first hit wire in the first PDC of this slide. We have looked closely at all 15 events with $E_{fit} - E_{egs} <$ -2 MeV on Fig.5c. From the EGS4 data 14 of these events lost more than 2 MeV in the first PDC pair of the selected slide, but this did not affect the overall accuracy of the track fit in the slide — the average value of the confidence level for these events was $\overline{CL_{14}} = 0.715$. The only event, #14252 has $CL = 0.033$. According to EGS4 this positron lost 2.1 MeV in the second plane of the second slide and the sliding method failed to find better slide because of too many kinks in the rest of the track. It means that sliding method gives statistically unreliable result with $CL = 0.033$ in 1 of 20000 events. Without sliding there were 3000 such events. Excluding the 14 events from Fig.5c but retaining event #14252 results in the spectrum presented on Fig.5d.

Vertex resolution $\sigma(X_{fit} - X_0, Y_{fit} - Y_0)$ varied from 0.24 mm to 0.08 mm at E_0=50 MeV and from 0.15 mm to 0.54 mm at E_0=20 MeV and θ_0 going from 10° to 60°.

Fig.6 presents the mean deviations of the fitted values $\overline{E_{fit}}$ and $\overline{\cos\theta_{fit}}$ as a function of initial angle θ_0. The values $\overline{\cos\theta_{fit} - \cos\theta_{egs}}$ do not exceed $6 \cdot 10^{-5}$ and the $\overline{(E_{fit} - E_{egs})}$ values are not more than 3 keV. The deviations of both values are essentially the same for simulated and reconstructed the helices at E_0=20 MeV and 35 MeV. Thus, the mean of the reconstructed positron helices will have a precision better than 4 keV for energy and better than $6 \cdot 10^{-5}$ for $\cos\theta$.

Energy and angular resolutions with and without multiple scattering were also calculated. The results are presented on Fig.7,8.

As it can be seen from Fig.7 the energy resolution becomes worse at $\theta < 20^\circ$. One obvious way to improve the energy resolution at small angles is to increase of the helium gap space between the PDC planes. We shall not examine it here. One can also expect to get better energy and angular resolution with Kalman filtering technique which takes into account multiple scattering effects. G.Lutz [4] gained a factor of 2 in momentum resolution of detector using the Kalman technique. Vacuum curves on Fig.7 display the limit that can be achieved.

Fig.9 shows the dependence of the mean reconstructed positron energy $\overline{E_{fit}}$ on $1/cos\theta$ value. As one can see, it can be parameterized with a linear function $\overline{E_{fit}} = E_0 - \alpha/\cos\theta$, where E_0 is the initial positron energy and α is the positron energy loss at $\theta = 0$ before entering a slide. The straight line fits to each slide data points are presented on Fig.9. The net result is: $\Delta \equiv \overline{E_{fit}} - E_0 = (-2.2 \pm 2)$ keV for extrapolation to $1/\cos\theta = 0$. We also checked this $\overline{E} = E_0 - \alpha/\cos\theta$ dependence at E_0=20 MeV and E_0=35 MeV and got $\Delta \equiv (-2 \pm 1)$ keV.

4.2 Continuous spectra reconstruction.

As it was shown above, $1/\cos\theta$ dependence allows to reconstruct initial positron energy and angle with adequate accuracy and this result is independent of the intrinsic accuracy of a simulation program. In this section we shall make use of this dependence want to obtain a response function for a continuous spectrum. Starting from the energy loss dependence valid for a planar detector $\Delta E(\theta) = \Delta E(\theta = 0)/\cos\theta \equiv \alpha/\cos\theta$ it is easy to derive a relation between the initial $M(E, \cos\theta)$ and final $\tilde{M}(\tilde{E}, \cos\tilde{\theta})$ distribution density functions

$$\tilde{M}(\tilde{E}, \cos\tilde{\theta}) = M(\tilde{E} + \frac{\alpha}{|\cos\tilde{\theta}|}, \cos\tilde{\theta}) \tag{3}$$

where E,θ and $\tilde{E}$,$\tilde{\theta}$ are positron energy and angle before and after passing through a planar degrader (assuming $\cos\tilde{\theta} = \cos\theta$).

We have applied this approach to the Michel spectrum of positrons from muon decay. The initial spectrum was generated in the form

$$M(x, \cos\theta) = \frac{\mathrm{d}^2\Gamma}{\mathrm{d}x\,\mathrm{d}\cos\theta} \equiv Nx^2 \Big\{ \Big[6(1-x) + \frac{4}{3}\rho(4x-3) + 6\eta x_0(1-x)/x\Big] - \\ -P_\mu\xi\cos\theta\Big[2(1-x) + \frac{4}{3}\delta(4x-3)\Big]\Big\} \tag{4}$$

where $x_0 = m_e/W$, $W = \frac{m_e^2+m_\mu^2}{2m_\mu}$, $x = E/W$. Michel parameters were set to standard $V-A$ values $\rho = \delta = 3/4$, $\eta = 0$, $P_\mu\xi = 1$.

Total statistics 10^9 decay events in 4π solid angle has been simulated with EGS4 for a real geometry of the detector (Fig.1) and $B = 2$ T with all interactions with matter taken into account. Positrons were emitted from a 2 cm diameter cylindrical volume in the stopped target (75 μm *Al* or 100 μm *Be*) with uniform coordinate distribution. Generated positrons were tracked in the range $0.38 < x < 1$, $0.4 < |\cos\theta| < 0.999$. Michel spectrum given by EGS4 at the entrance to PDC(+1X) and PDC(-1X) was then fitted in the range $0.45 < x < 0.9$, $0.5 < |\cos\theta| < 0.985$ to a function (4) with substitution made $x \to \tilde{x} + \alpha/|\cos\theta|$ Parameter α was varied in fit together with other parameters N, ρ, η, $P_\mu\xi$, δ. Fit results are presented in Table 2.

We have used the most simple form of response function (3) which only accounts for an energy shift of a whole spectra at certain polar angle θ due to average energy losses of positron in the stopped target, chambers and He gap. The energy losses dependence on energy was not taken into account. However, a linear function $\Delta E(E, \theta) = (\alpha + \beta E)/\cos\theta$ is a good approximation for energy losses of positron in the range $E = 20 \div 60$ MeV as it is demonstrated on Fig.10 (data taken from [5]), and this energy dependence of energy losses can to be included in a more sophisticated calculation of the response function. We have also made an assumption that the mean value of $\cos\theta$ is conserved in positron interactions with matter, but this is only approximately true as can be seen from Fig.11. Non-conservation of $\overline{\cos\theta}$ is a result of positron scattering because after scattering $\overline{\cos\theta} \neq \cos\overline{\theta}$. This effect must also be included in response function. We have not taken into account big energy losses of positron due to both radiative processes and large fluctuations of ionization losses. The distortion of initially flat energy distribution due to these effects are illustrated on Fig.12.

So, it has been shown in this section that the simple response function taking into account only the average energy losses of positron in the range $E = 20 \div 50$ MeV and making use of $1/\cos\theta$ dependence allows to substantially reduce systematic shifts of Michel parameters and does not require the actual knowledge of the value of the average energy losses in detector.

4.3 Lorentz drift angle.

In previous sections 4.1, 4.2 the possibility to reconstruct with high precision a *true* mean *original* energy as well as continuous spectrum parameters in a detector featuring a $1/\cos\theta$ dependence of average energy losses in all detector components has been demonstrated. The example PDC assembly based detector considered above is not the only possible detector scheme having this dependence, so, in principle, similar technique can be applied for other types of detectors too. TPC based detectors are obvious candidates. Nevertheless, other factors specific for a particular detector can become obstacles for achieving the goal. The full analysis of the effect of numerous possible sources of systematic errors in real-life detectors (like wire positions accuracy, drift velocity dependence on gas temperature and pressure, detector misalignment with respect to magnetic field direction, magnetic field instability and homogeneity and so on) on particle track reconstruction is beyond the scope of this paper. We shall consider here only the influence of Lorentz drift effect.

In the presence of magnetic field drift path lengthening due to Lorentz drift effect changes the STR (space-time relation) of a drift cell. If this change of STR is not taken into account in track reconstruction the reconstructed spectra can be considerably distorted. It was demonstrated for TPC case in [7]. We shall analyze this effect for the proposed spectrometer (See Fig.1) with DME gas at B=2 T. In this case maximum Lorentz drift angle value does not exceed $\theta_{L,max} = 9°$ [8] and average θ_L is less then $4°$ in the drift cell. Nevertheless, we shall conservatively use in estimates a maximum drift angle value $\theta_{L,max} = 9^{\circ}$.

The following simplified simulation model was used. Distances of closest approach of vacuum helix to hit wires d_i (*DOCA*s) were calculated first. Local Lorentz drift angles at the points of closest approach was then computed to take into account the dependence of Lorentz drift component on the angle between electric $\overrightarrow{\mathcal{E}}$ and magnetic $\overrightarrow{B}$ field $\theta_L \approx \theta_{L,max}|\sin(\widehat{\overrightarrow{\mathcal{E}}, \overrightarrow{B}})|$ under the assumption of a constant (maximum) Lorentz angle and simple radial direction of electrostatic field in PDC cell. Finally, true *DOCA*s d_i were replaced in $\chi^2 = \sum_{i=1}^{N_{hits}} \frac{(d-d_i)^2}{\sigma_i^2}$ by longer drift distances $d_{i,L}$ corresponding to Lorentz angle values $d_{i,L} = d_i / \cos\theta_{i,L}$ and smeared with gaussian PDC resolution and modified $\chi_L^2 = \sum_{i=1}^{N_{hits}} \frac{(d-d_{i,L})^2}{\sigma_i^2}$ was minimized to find parameters $(R_0, k_0, \phi_0, X_a, Y_a)$ of track (1). Only the first 4 PDC pairs were used in track fit and sliding technique was not applied.

To avoid masking the Lorentz drift effect on track reconstruction PDC resolution in simulation was assumed to be σ_{PDC}=0.5 μm instead of a realistic 50 μm value. Results for the mean deviation of reconstructed energy $\overline{\Delta E} = \overline{E_{fit} - E_0}$ are presented on fig.13. As one can see from fig.13, maximum deviations $|\overline{\Delta E}| \approx 100$ keV are observed at small polar angles $\theta = 9.9^{\circ}$ ($\cos\theta = 0.985$) when positrons are emitted from a point source ($\sigma_{x_0} = \sigma_{y_0} = 0$) at a fixed polar angle ($\phi_0 = 0$). The mean energy deviation drops drastically ($|\overline{\Delta E}| \leq 5$ keV at $\cos\theta = 0.985$) due to averaging when one considers a distributed gaussian source spot ($\sigma_{x_0} = \sigma_{y_0}$ =1 cm, $\phi_0 = 0$). For a smaller Lorentz angle value $\theta_{L,max} = 3^{\circ}$ (or, equivalently, if one corrects drift distances in STR for Lorentz drift with 10% accuracy) the same average over source spot ($\sigma_{x_0} = \sigma_{y_0} = 1$ cm, $\phi_0 = 0$) gives $|\overline{\Delta E}| \leq 0.6$ keV. $\overline{\Delta E}$ becomes negligible at $\cos\theta \leq 0.9$. Similarly, deviation of reconstructed polar angle is maximal for point source and fixed azimuthal angle ($|\overline{\Delta \cos\theta}| = |\overline{\cos\theta - \cos\theta_0}| \approx 7 \cdot 10^{-5}$ at $\cos\theta = 0.985$ and $\sigma_{x_0} = \sigma_{y_0} = 0$, $\phi_0 = 0$) and drops to $|\overline{\Delta \cos\theta}| \leq 2 \cdot 10^{-6}$ for distributed source $\sigma_{x_0} = \sigma_{y_0} = 1$ cm, $\phi_0 = 0$. For Lorentz angle $\theta_{L,max} = 3^{\circ}$ this deviation becomes $|\overline{\Delta \cos\theta}| \leq 2 \cdot 10^{-7}$.

A closer look at fit results (See Fig.14,15) reveals sophisticated regular patterns of fitted energy which reflect a periodic structure of the detector. PDC drift cells 4 mm periodicity is clearly seen on Fig.15. Interestingly, there is practically no change in figures for mean energy and angle deviations in case of realistic PDC resolution 50 μm, even though detector energy resolution goes from few 100 keV to 1 MeV and fine pattern structure is hidden. (see last scatterplot on Fig.14). On the other hand, averaging over uniform in 2π azimuthal distribution of ϕ_0 results in reduction of $|\overline{\Delta E}|$ and $|\overline{\Delta \cos\theta}|$ comparable to averaging over x_0, y_0. The systematic shift of mean reconstructed energy demonstrated above if not corrected is translated directly to a shift of any narrow energy peak one can be interested in. The Lorentz drift effect can also distort continuous spectra.

Fig.16 presents the reconstructed energy spectrum, the original spectrum was flat in the range $E_0 = 20 \div 50$ MeV, $\sigma_{x_0} = \sigma_{y_0} = 0$, $\phi_0 = 0$. Total number of simulated events was 10^5. For an isotropic original spectrum this would correspond to a full statistics $> 10^{12}$ in 4π solid angle. As one can see from Fig.16, χ^2 values in all cases are significantly beyond their natural limits $\chi^2 = ndf \pm \sqrt{2\,ndf}$, i.e. systematic errors in spectrum are higher than statistical errors. χ^2 values for distributed source ($\sigma_{x_0} = \sigma_{y_0} = 1$ cm, $\phi_0 = 0$) are within their natural limits, indicating that systematic errors from Lorentz drift effect are small at total statistics 10^{12} in 4π angle.

4.4 Positive ion effect estimation.

Positive ions produced near PDC anodes in the avalanche process induce electric field distortions in PDC cell that may in turn change STR. This effect was estimated for TPC in [9]. We apply its results (see [9],p.83) to estimate electric field reduction due to space–charge effects. For a minimum ionizing particle flux $I = 300$ mm^{-2}s^{-1} relative electric field change $\Delta\mathcal{E}/\mathcal{E}$ is less than 10^{-3}. Flux distribution was considered to be uniform, gas gain was taken to be $5 \cdot 10^3$, average field in PDC — $\mathcal{E} = 1kV/mm$ and ion mobility of DME gas — 0.3 cm^{2}V^{-1}s^{-1}. Since in DME gas $v_{drift} \propto \mathcal{E}$ ([10]) field reduction $\Delta\mathcal{E}/\mathcal{E} = 10^{-3}$ corresponds to drift path lengthening $\Delta l/l \approx 10^{-3}$. Shifts of $\overline{\Delta E}$, $\overline{\Delta \cos\theta}$ and continuous spectrum distortions can be estimated with a technique similar to the one used in section 4.3. For example, at $\cos\theta_{L,max} = 3°$ relative drift path change is $\Delta l/l = 1.4 \cdot 10^{-3}$. Hence, at $I = 300$ mm^{-2}s^{-1} shifts of mean reconstructed energy and angle as well as systematics in continuous spectrum are negligible for total statistics $< 10^{12}$ in 4π (as it was shown for $\cos\theta_{L,max} = 3°$ case in section 4.3). Note that we have applied results for a uniform $\mathcal{E}$ field to get the estimates above, which is, obviously, not the case for PDC cell. More accurate analysis of positive ion influence on a spectrometer precision must be done with more detailed PDC design. For example, in case of PDC cells without field wires, as in [11], positive ions may tend to concentrate in $\mathcal{E} \approx 0$ areas of PDC cell and their effect on STR can be stronger.

5 Conclusions.

We have shown with Monte-Carlo simulation, that magnetic spectrometer with a planar target and planar drift chambers arranged perpendicularly to the magnetic field allows to reconstruct with high precision *original* mean energy of mono-energetic particles emitted from target. In a sample detector

(Fig.1, Table 1) for positrons with initial energy in the range $20 \div 50$ MeV this can be done with accuracy $\overline{\Delta E} \simeq 2$ keV without making any assumptions about energy loss even though typical positron energy loss in target and chambers is more than 100 keV. EGS4 simulation computes all types of positron interactions in detector including big energy loss in radiative processes. Naturally, simulation precision of EGS4 is not absolute, but the achieved energy reconstruction accuracy $\overline{\Delta E} \simeq 2$ keV does not depend on simulation accuracy. It is also independent of the spatial distribution of source in the target.

The accuracy of continuous spectrum reconstruction in suggested detector has been demonstrated on the example of the differential spectrum of positrons from $\mu \to e\nu\tilde{\nu}$ decay. It is shown for a full statistics of 10^9 $\mu \to e$ decays in 4π that systematic errors of reconstructed Michel parameters do not exceed 10^{-3} for parameters ρ, δ and$P_\mu\xi$ and $6 \cdot 10^{-2}$ for parameter η. To reduce these errors one has to take into account non-conservation of $\overline{\cos\theta}$ in scattering, energy loss dependence on energy and distortions of continuous spectrum because of large energy loss events. Obviously, this can only be done with finite accuracy. For example, if a simulation package works with $\pm 4\%$ accuracy, systematic errors in parameters ρ, δ, $P_\mu\xi$ can be lowered to $< 10^{-4}$ level and in parameter η — to $3 \cdot 10^{-3}$. Of course, systematic errors depend of the spectrum being studied.

The suggested sliding technique allows to find track segment with minimum scattering/energy loss and to achieve statistically significant track reconstruction with $\overline{CL} > 0.5$. The disadvantage of this approach is the necessity to increase (about two times) the number of detector channels.

The Lorentz drift effect on reconstruction accuracy has been investigated. Maximum value of $\theta_L = 9°$ for DME gas in 2 T field was used in estimates. If Lorentz drift is not taken into account maximum reconstruction errors are observed for small polar angles $\theta \simeq 10°$ ($\cos\theta = 0.985$). Mean reconstructed energy shift reaches $\overline{\Delta E} \sim 100$ keV for particles emitted at fixed polar and azimutal angles from a point source. Averaging over distributed 1 cm origin source and/or averaging over azimutal angle $\phi_0 = 0 - 2\pi$ takes this error down to less than 5 keV. At polar angles $\theta > 10°$ all these distortions are much smaller. It is shown, that χ^2 value for reconstructed flat energy spectrum corresponding to total statistics 10^{12} in 4π solid angle is far beyond statistical limits for an unaveraged spectrum while the averaging results in statistically significant $\chi^2 = ndf \pm \sqrt{2\,ndf}$ value.

Estimate has been done on positive ion effect on reconstruction accuracy. It is shown, that beam intensity 300 $\mathrm{s}^{-1}\mathrm{mm}^{-2}$ for PDC cell with nonsaturated DME gas causes negligible errors of track reconstruction.

Acknowledgement

We would like to thank A.Astbury and S.T.Belyaev for their support of the TRIUMF experiment 614. We are thankfull to D.Gill who read the manuscript and whose remarks helped make it better. We would like to thank M.Comyn, Y.Davydov, C.Gagliardi, P.Gumplinger, J.A.MacDonald, J.-M.Poutissou, R.Poutissou, V.Torokhov, B.Tribble, D.Wright for many useful discussions.

References

[1] Y.Y.Lachin, L.V.Miassoedov,I.V.Morozov, V.I.Selivanov, I.V.Sinitzin, V.D.Torokhov, Nucl.Instr. and Meth., A361(1995)77–84

[2] R.W.Hockney, W.Roger, “Computer simulation using particles”, New York, 1988.

[3] R. Fruhwirth, Nucl.Instr. and Meth. A262 (1987)444-450

[4] G.Lutz, Nucl.Instr. and Meth. A273(1988)349-361

[5] M.J.Berger, S.M.Seltzer, “Tables of Energy Losses and Ranges of Electrons and Positrons”, National Academy of Sciences (National Research Council, Washington, D.C.) Publication 1133(1964)205.

[6] M.J.Berger, ‘Electron Stopping Powers for Transport Calculations” in “Monte Carlo Transport of Electrons and Photons”, editors T.M.Jenkins, W.R.Nelson, A.Rindi, Plenum Press, 1986, p.p. 57-77.

[7] Ming-Jen Yang, Nucl.Instr. and Meth. A270(1988)126-139.

[8] B.Zhou, A.Marin, T.Coan, J.Beatty, S.Ahlen, Nucl.Instr. and Meth. A287(1990) 439-446.

[9] D.Friederich, G.Melchart, B.Sadoulet, F.Sauli, Nucl.Instr. and Meth. 158(1979)81-88.

[10] F.Villa, Nucl.Instr. and Meth. 217(1983)273-276.

[11] V.Cindro, H.Kolanski, A.Lange, D.Lauterjung, F.Miller, T.Siegmund, W.Soder, H.Thurn, Nucl.Instr. and Meth. A309(1991)411-421.

Table 1
The PC and PDC specification.

	PC	PDC
diameter of $(W(Re))Au$ sense wire	12.7 μm	
diameter of $(CuBe)Au$ field wire	—	25.4 μm
distance between sense wires	2 mm	4 mm
distance between sense and field wires	—	2 mm
distance between sense wire plane and H.V.plane	2 mm	
H.V. plane	double-side, 6 μm aluminized mylar	
drift gas	$CF_4/ISO(80/20)$	DME (C_2H_6O)
pressure	760 torr	
temperature	20° C	

Table 2
Fitted values of Michel parameters.

Target	α $\pm stat.err.$ (10^{-4})	$(0.75-\rho)$ $\pm stat.err.$ (10^{-4})	η $\pm stat.err$ (10^{-2})	$(1-P_\mu\xi)$ $\pm stat.err.$ (10^{-4})	$(0.75-\delta)$ $\pm stat.err.$ (10^{-4})
Be	0 (fixed)	0.5 ± 5.7	12.9 ± 3.1	-52.7 ± 5	13.9 ± 1.9
	6.6 ± 0.9	0.6 ± 5.7	2.9 ± 3.4	4.4 ± 9.2	-0.4 ± 2.7
Al	0 (fixed)	4.7 ± 5.7	17.4 ± 3.1	-67.2 ± 5	24 ± 1.9
	7.0 ± 0.9	5.9 ± 5.7	6.7 ± 3.4	-6.5 ± 9.2	9.6 ± 2.7

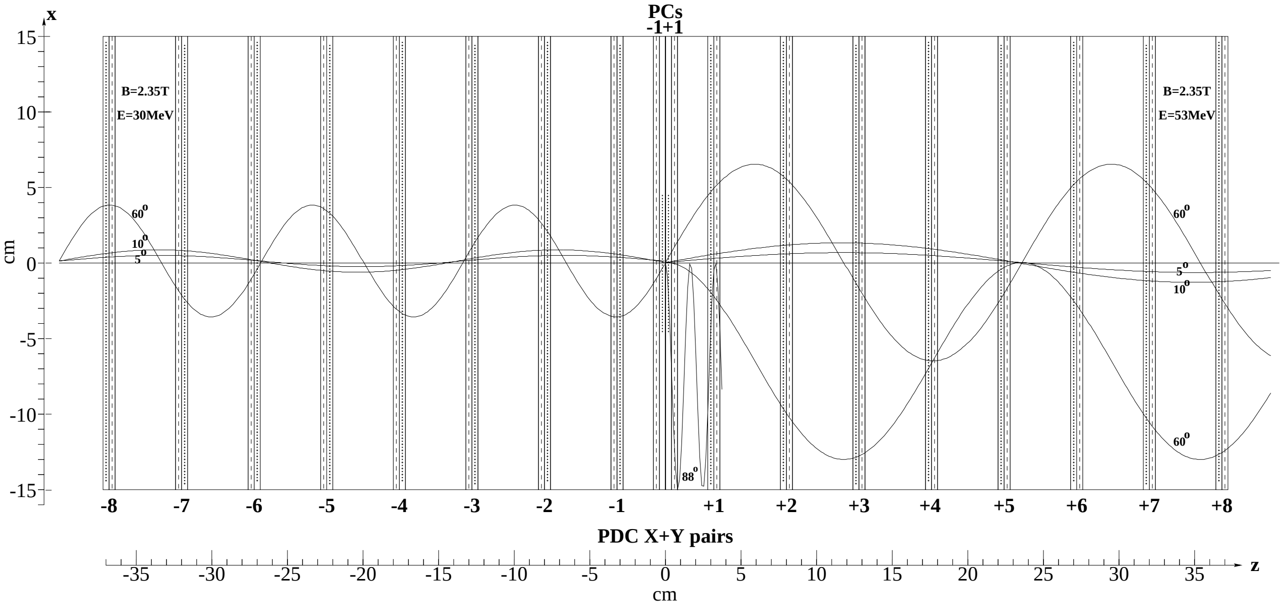

Fig. 1. Schematic layout of detector assembly.

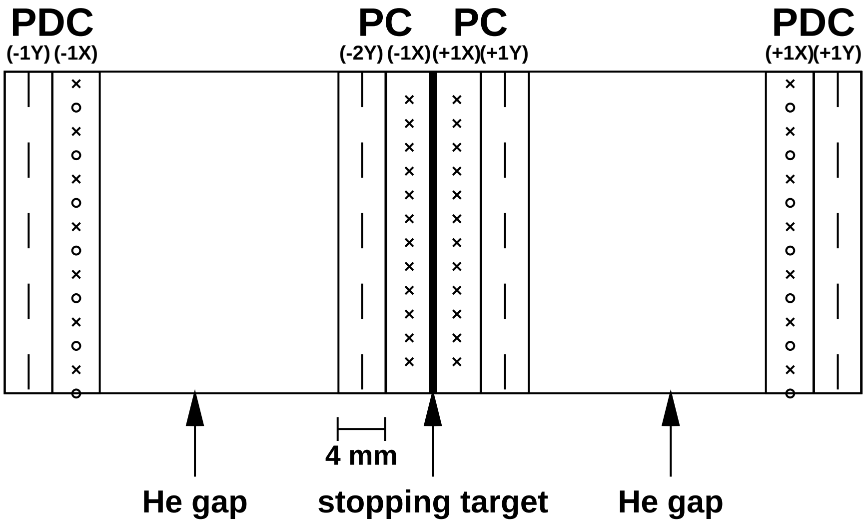

Fig. 2. Central part of the detector. Gas gap of both the PCs and the PDCs equals to $4mm$. Sense wires in both the PCs and the PDCs are 12.7 μm gold covered tungsten. Field wires in the PDCs are 25.4 μm gold covered $Cu(Be)$ alloy. Helium gap is 20 mm. Magnetic field direction is perpendicular to the chamber planes.

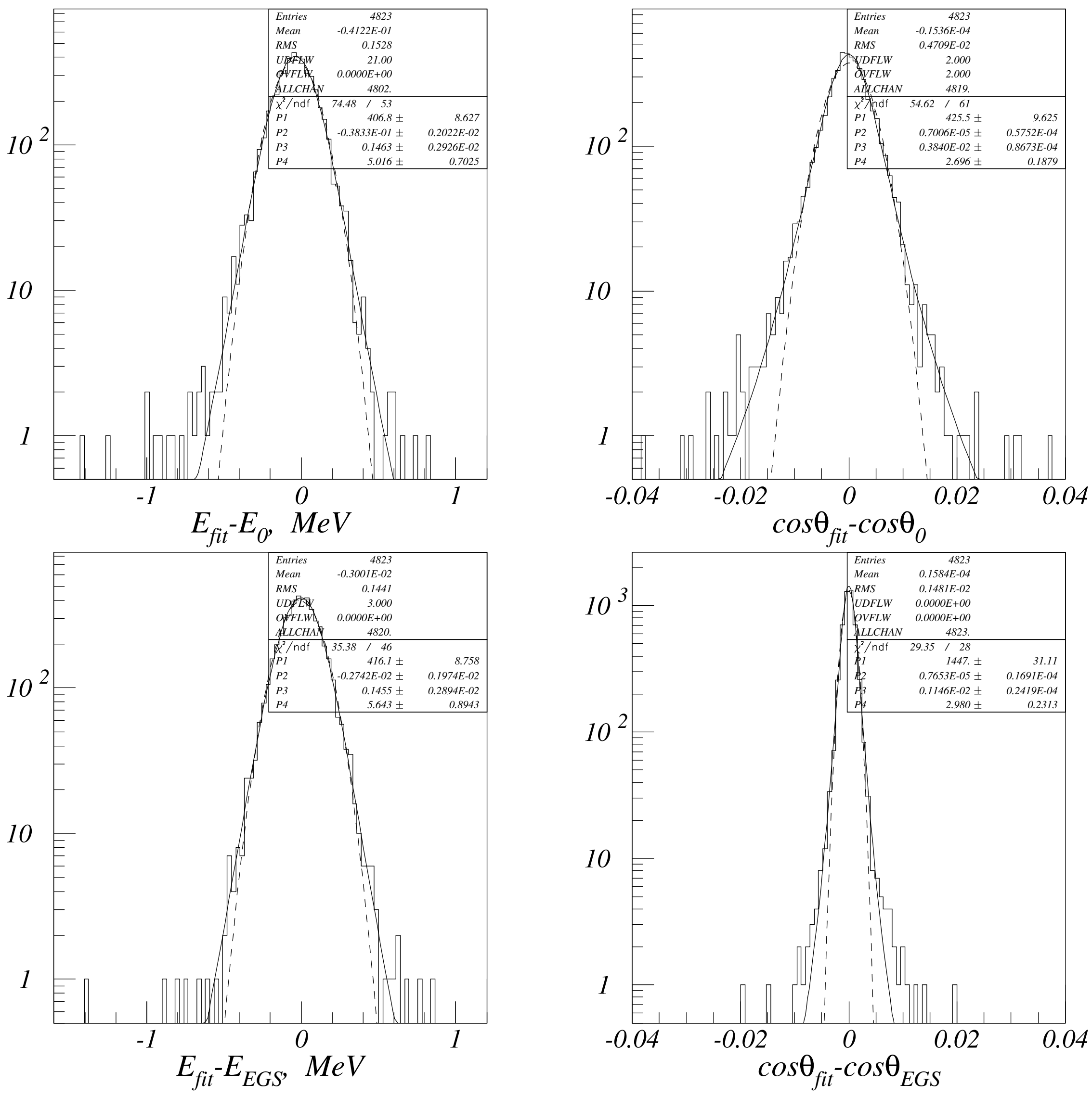

Fig. 3. Reconstructed distributions of E_{fit} and $\cos\theta_{fit}$ fitted by the generalized Breit-Wigner (solid curve) and the Gaussian (dashed curve) functions for the 1st slide data. $P1 = \alpha$, $P2 = \overline{x}$, $P3 = \gamma = HWHM$, and $P4 = \beta$ are the parameters of the Breit-Wigner. $E_0 = 50$ MeV, $\cos\theta_0 = 0.735$, PDC resolution 50 μm.

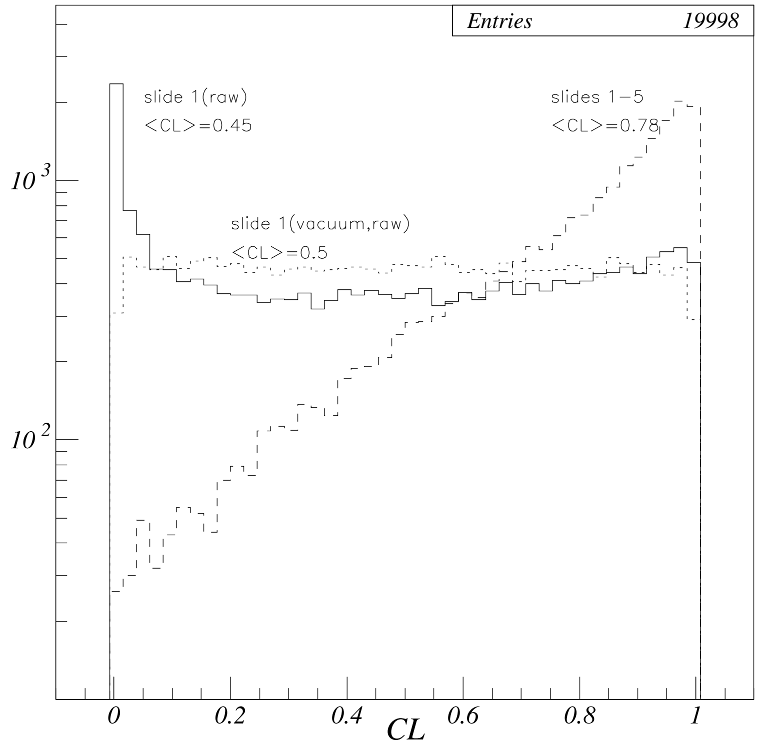

Fig. 4. Confidence level (CL) distribution for reconstructed events. Initial positron energy $50MeV$, initial polar angle $\cos\theta_0 = 0.735$. PDC space resolution is 50 μm. "Raw" is the result of the first slide (*1234*) fitting. "Slides" present the same events which were fitted with slide selection and the resulting distributions of all five slides were summed. The flat distribution with $\overline{CL} = 0.5$ corresponds to the fit of vacuum helices with 50 μm PDC resolution.

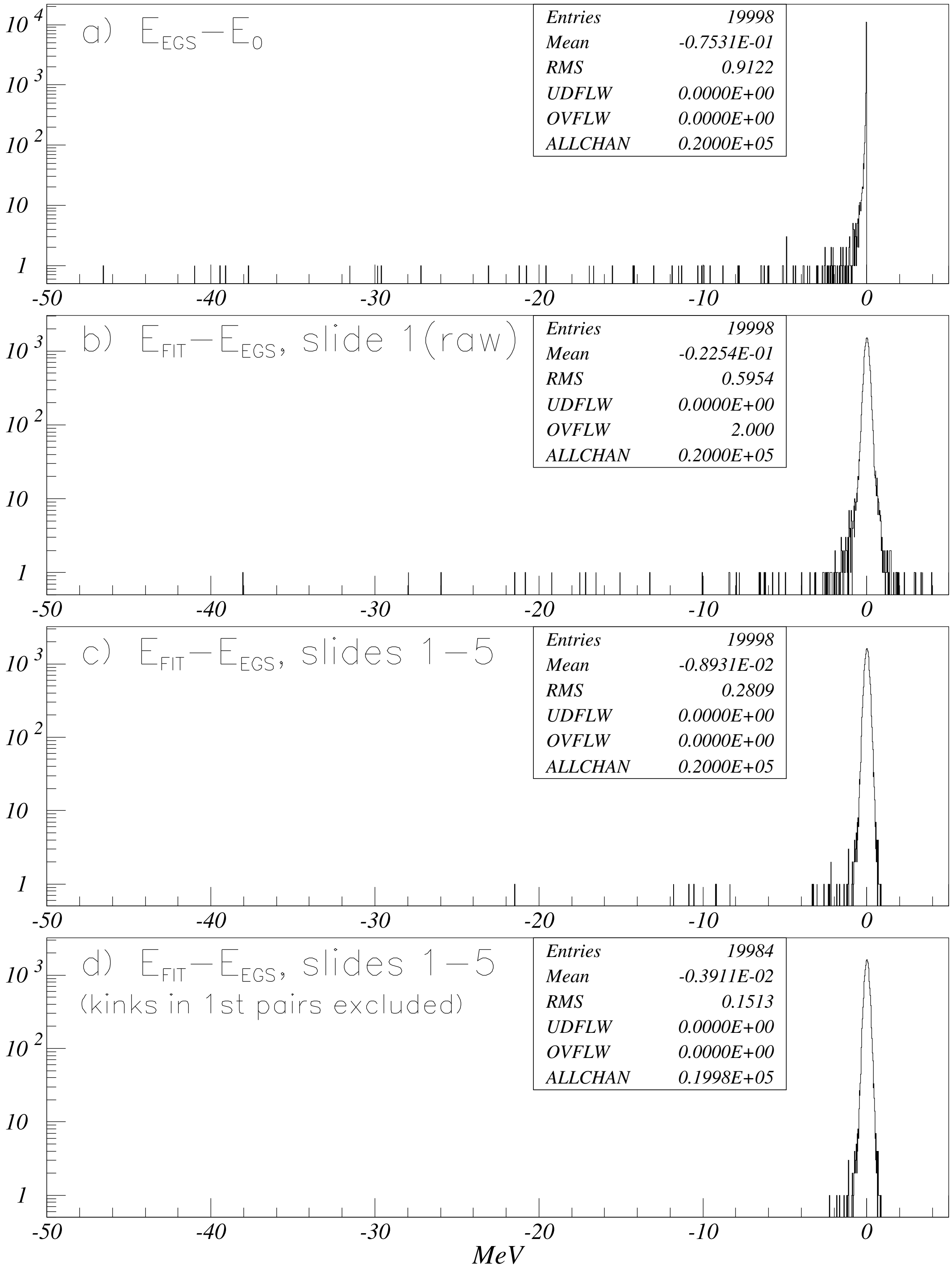

Fig. 5. Energy distributions of positrons in detector. E_0 is initial positron energy in the target. E_{EGS} is positron energy in the first PDC pair of the corresponding slide. E_{FIT} is the positron energy found by the reconstruction program. E_0=50 MeV, $\cos\theta_0 = 0.735$, PDC resolution 50 μm.

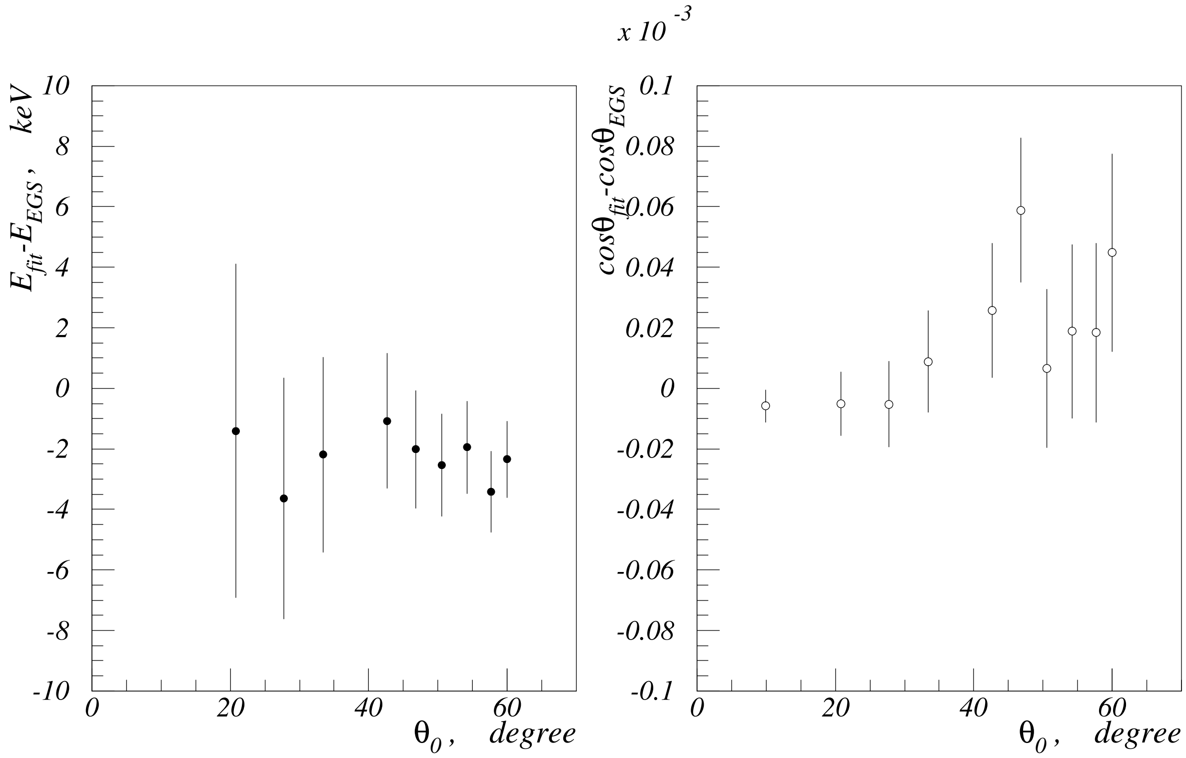

Fig. 6. Mean deviation of the fitted values $\overline{(E_{fit} - E_{egs})}$ and $\overline{(\cos\theta_{fit} - \cos\theta_{egs})}$ as a function of initial polar angle θ_0 at E_0=50 MeV (5th slide data). E_{egs} and $\cos\theta_{egs}$ are the values given by EGS4 in the first PDC of the 5th slide. E_{fit} and $\cos\theta_{fit}$ are the fitted values in the same PDC.

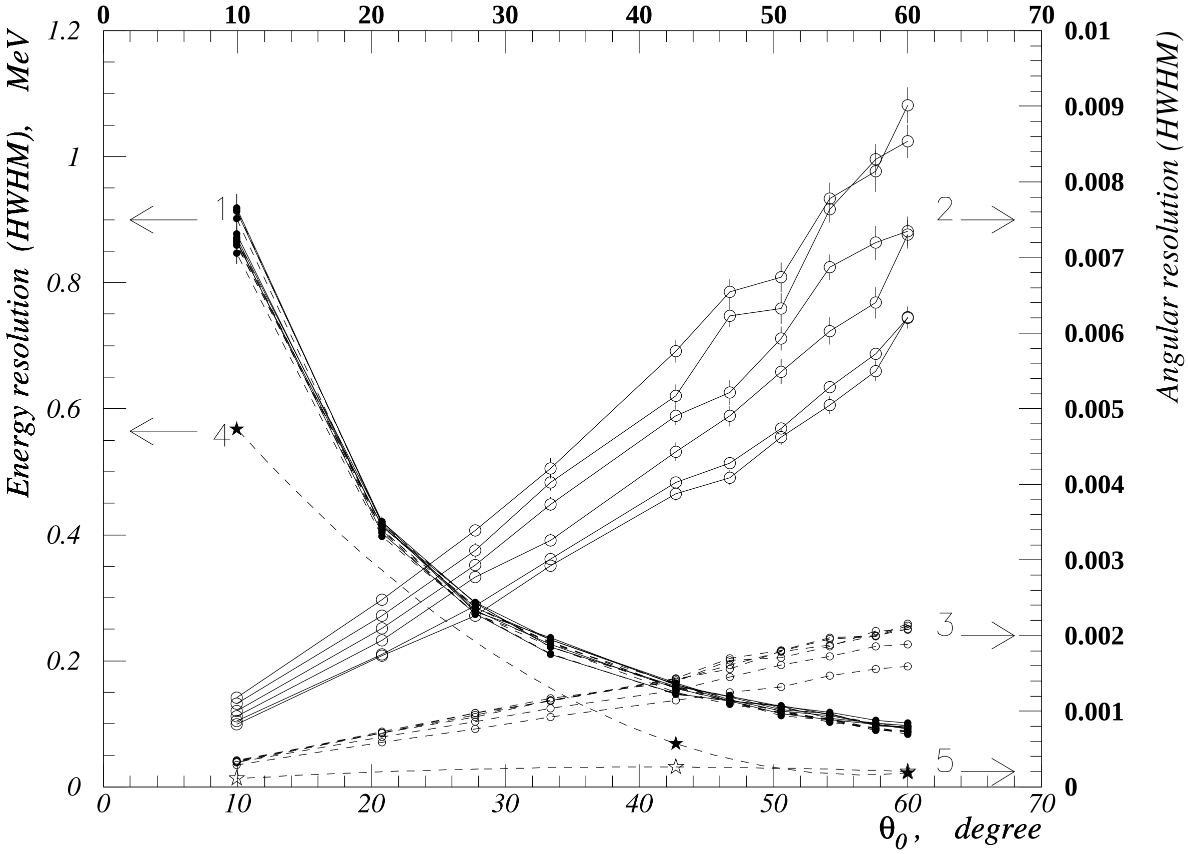

Fig. 7. Energy and angle resolution of the detector versus angle θ_0 at E_0=50 MeV, PDC resolution 50 μm.
1) – $HWHM(E_{fit} - E_0)$(solid), $HWHM(E_{fit} - E_{egs})$(dashed) – all slides;
2) – $HWHM(\cos\theta_{fit} - \cos\theta_0)$, (all slides);
3) – $HWHM(\cos\theta_{fit} - \cos\theta_{egs})$, (all slides);
4) – $HWHM(E_{fit} - E_0)$ for vacuum helices(no scattering);
5) – $HWHM(\cos\theta_{fit} - \cos\theta_0)$ for vacuum helices(no scattering).

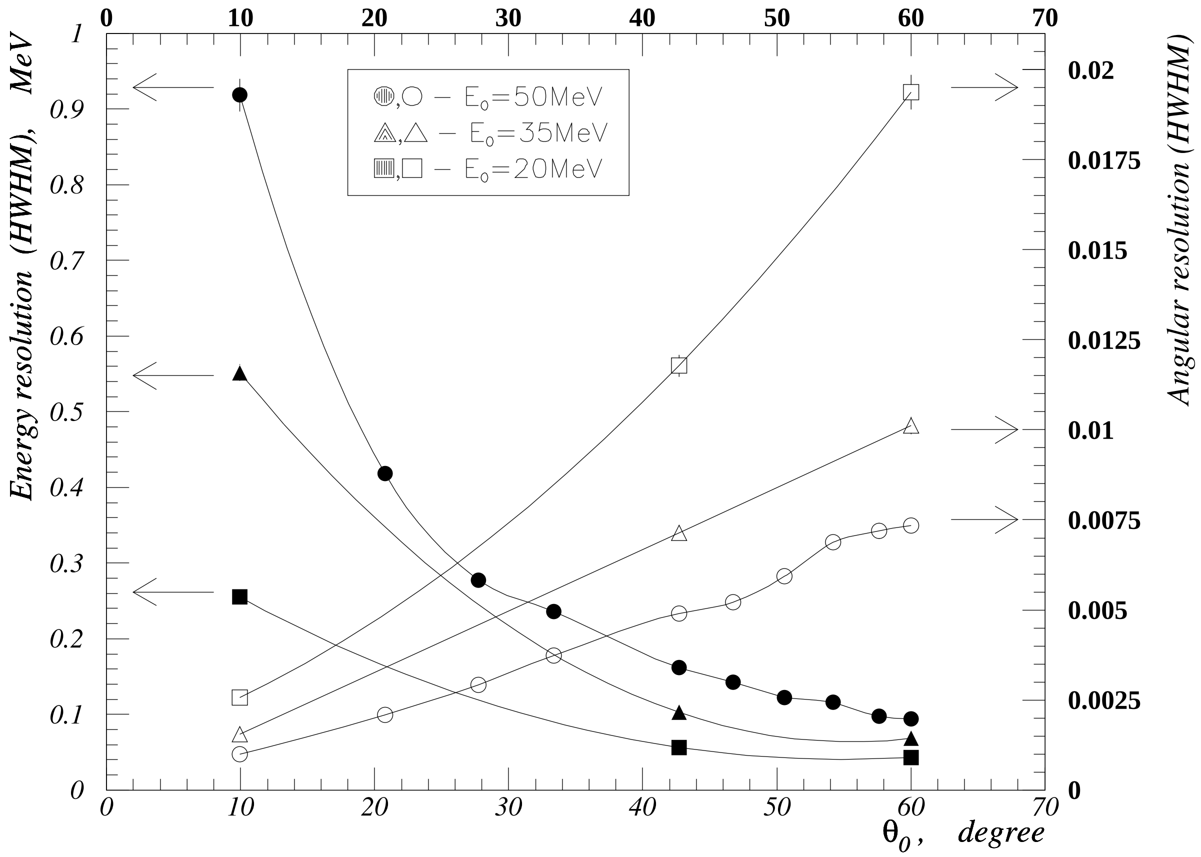

Fig. 8. Energy $HWHM(E_{fit} - E_0)$ and angle $HWHM(\cos\theta_{fit} - \cos\theta_0)$ resolutions at different initial energies of positron. 3rd slide data only. PDC resolution is 50 μ m.

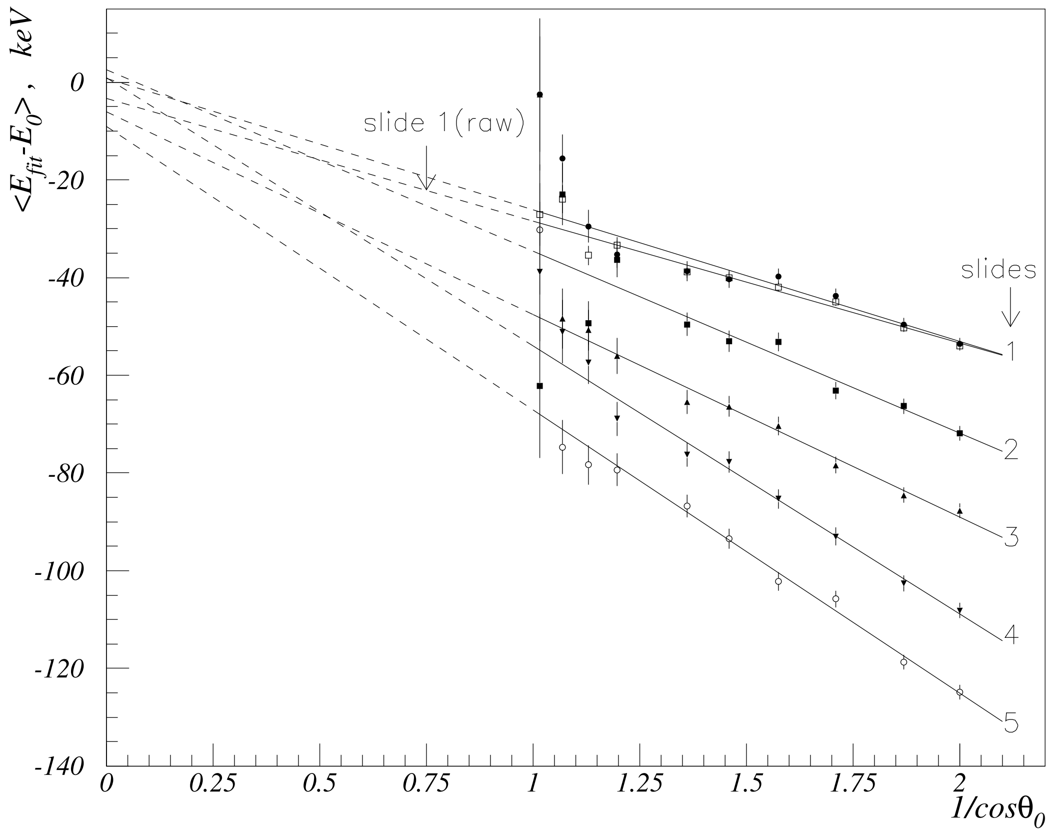

Fig. 9. Mean reconstructed positron energy $\overline{E_{fit}}$ as a function of $1/\cos\theta$. E_0=50 MeV, σ_{PDC}=50 μm. Straight lines are the fits with function $\overline{E_{fit}} = E_0 - \alpha/\cos\theta$.

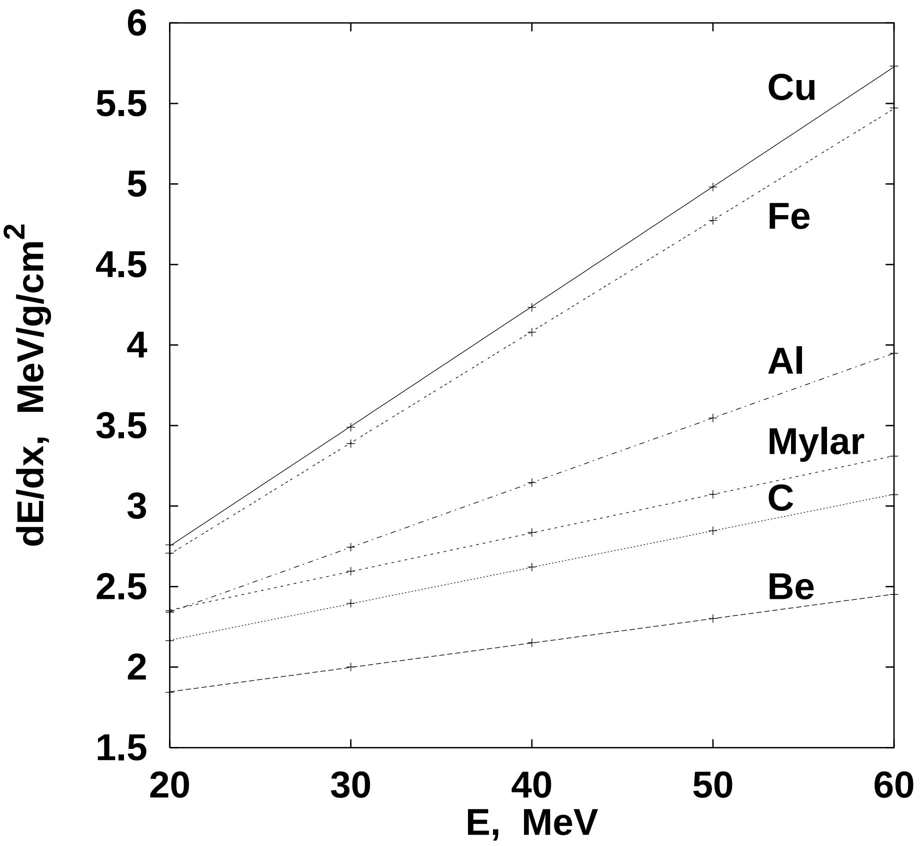

Fig. 10. Stopping power for positron in several materials.

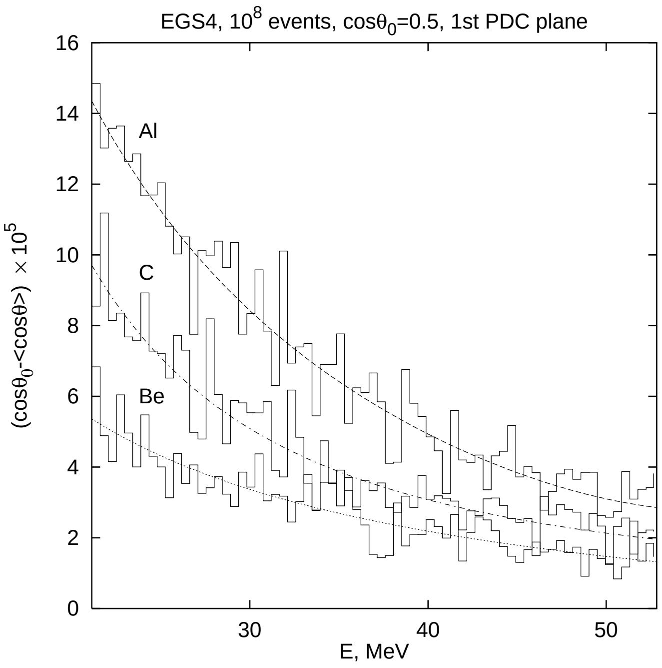

Fig. 11. Non-conservation of $\overline{\cos\theta_{egs}}$ for different target materials. Initial positron energy distribution in target was uniform in the range 20 MeV$<$ E_0 $<$52.83 MeV. Initial $\cos\theta_0 = 0.5$. Targets thickness: Al – 75 μm, Be – 100 μm, C – 100 μm. For cases with Be and C targets 15 μm diameter Fe sense and field wires were taken. 10^8 events were generated for each target.

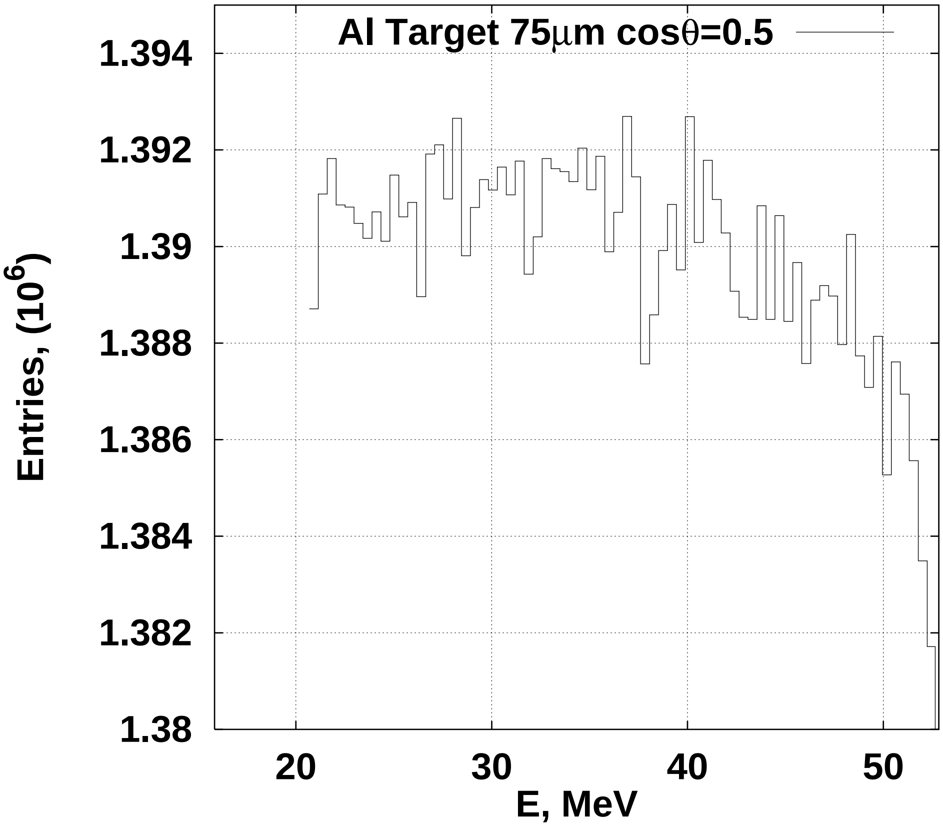

Fig. 12. Energy spectrum (EGS4 simulation) for Al target at the entrance to PDC(+1X). Initial spectrum was sampled from the uniform distribution in the range 16 MeV$\leq E_0 \leq 52.83$ MeV, $\cos\theta = 0.5$, B=2 T, positron source was uniformly distributed in 2 cm diameter cylindrical volume in the target, total statistics 10^8 decay events.

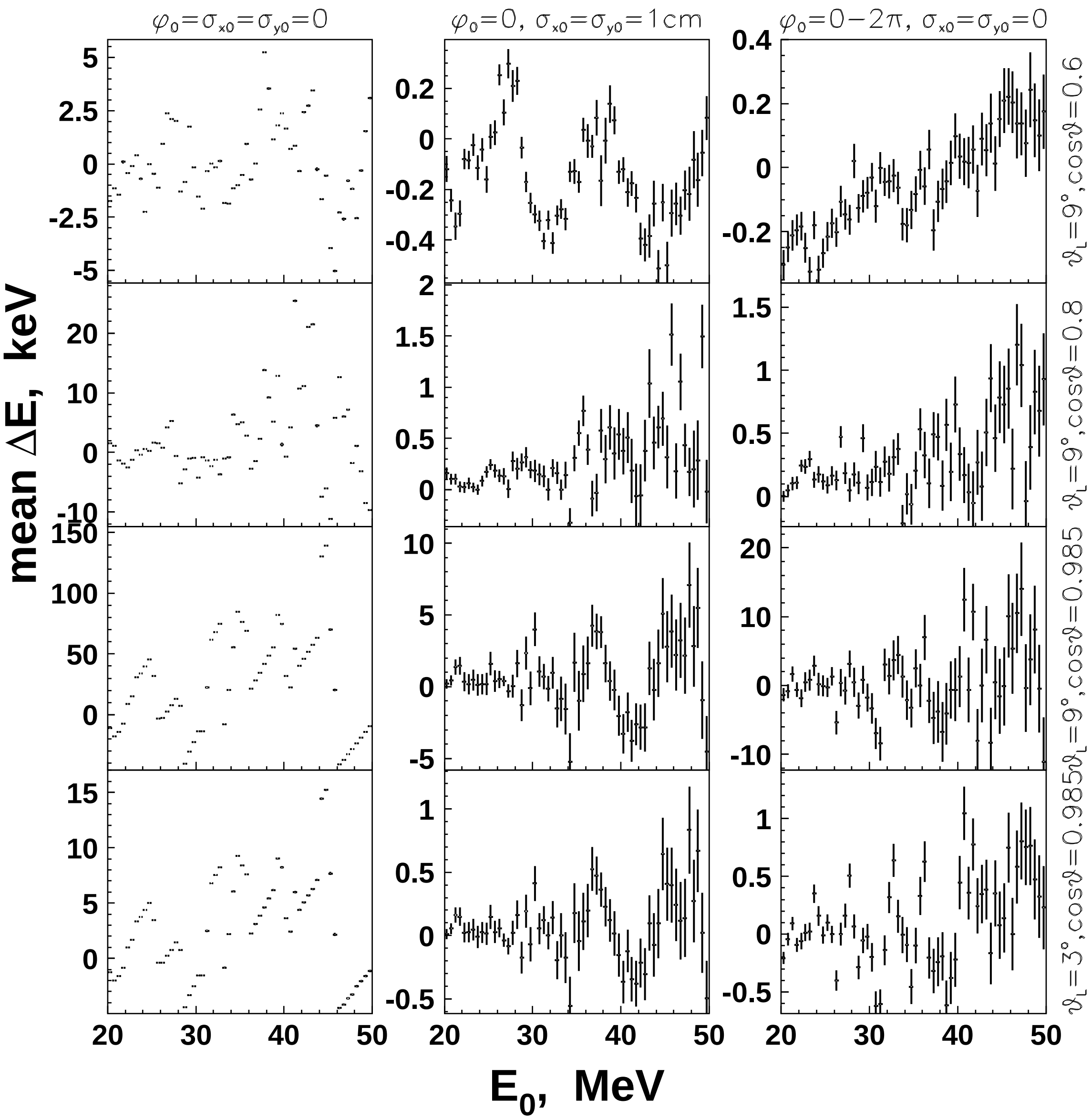

Fig. 13. Mean shift of fitted energy $\overline{\Delta E} = \overline{E_{fit} - E_0}$ as a function of initial energy E_0.

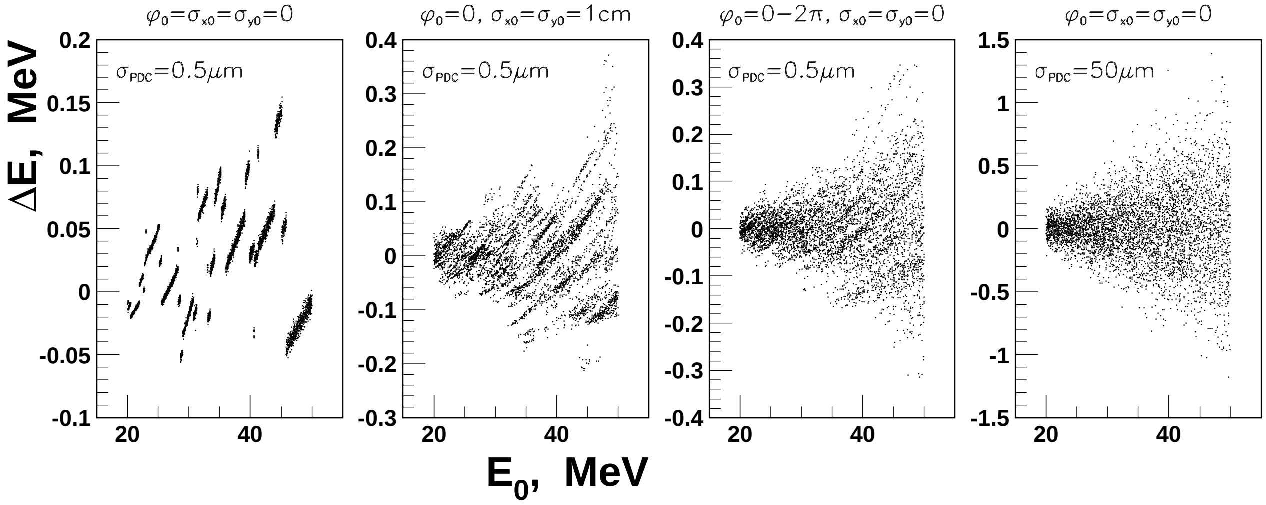

Fig. 14. Scatterplot of fitted energy shift $\Delta E = E_{fit} - E_0$ versus initial energy E_0 at $\cos\theta = 0.985$, $\theta_{L,max} = 9^{\circ}$.

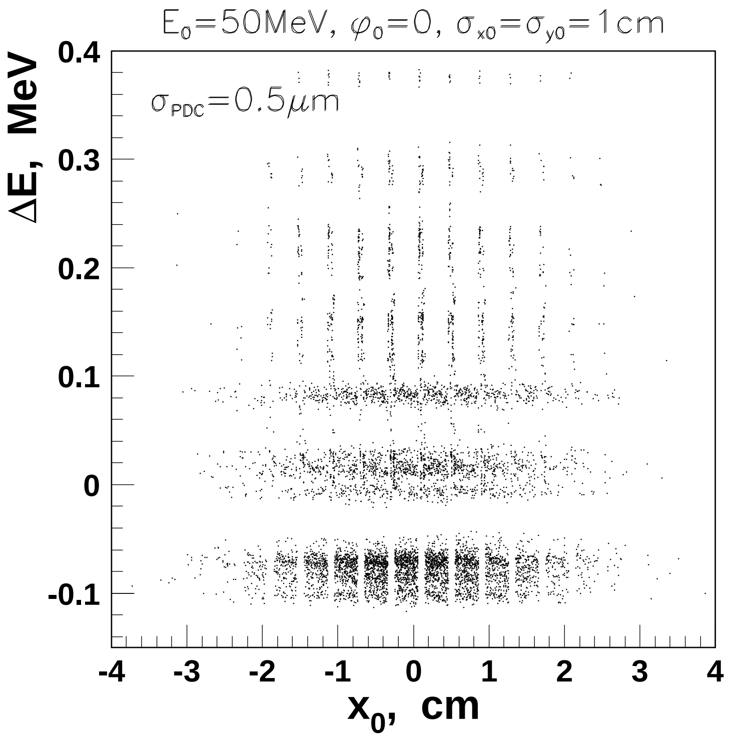

Fig. 15. Scatterplot of fitted energy shift $\Delta E = E_{fit} - E_0$ versus positron origin x_0 for initial energy $E_0 = 50$ MeV and $\cos\theta = 0.985$, $\theta_{L,max} = 9^{\circ}$.

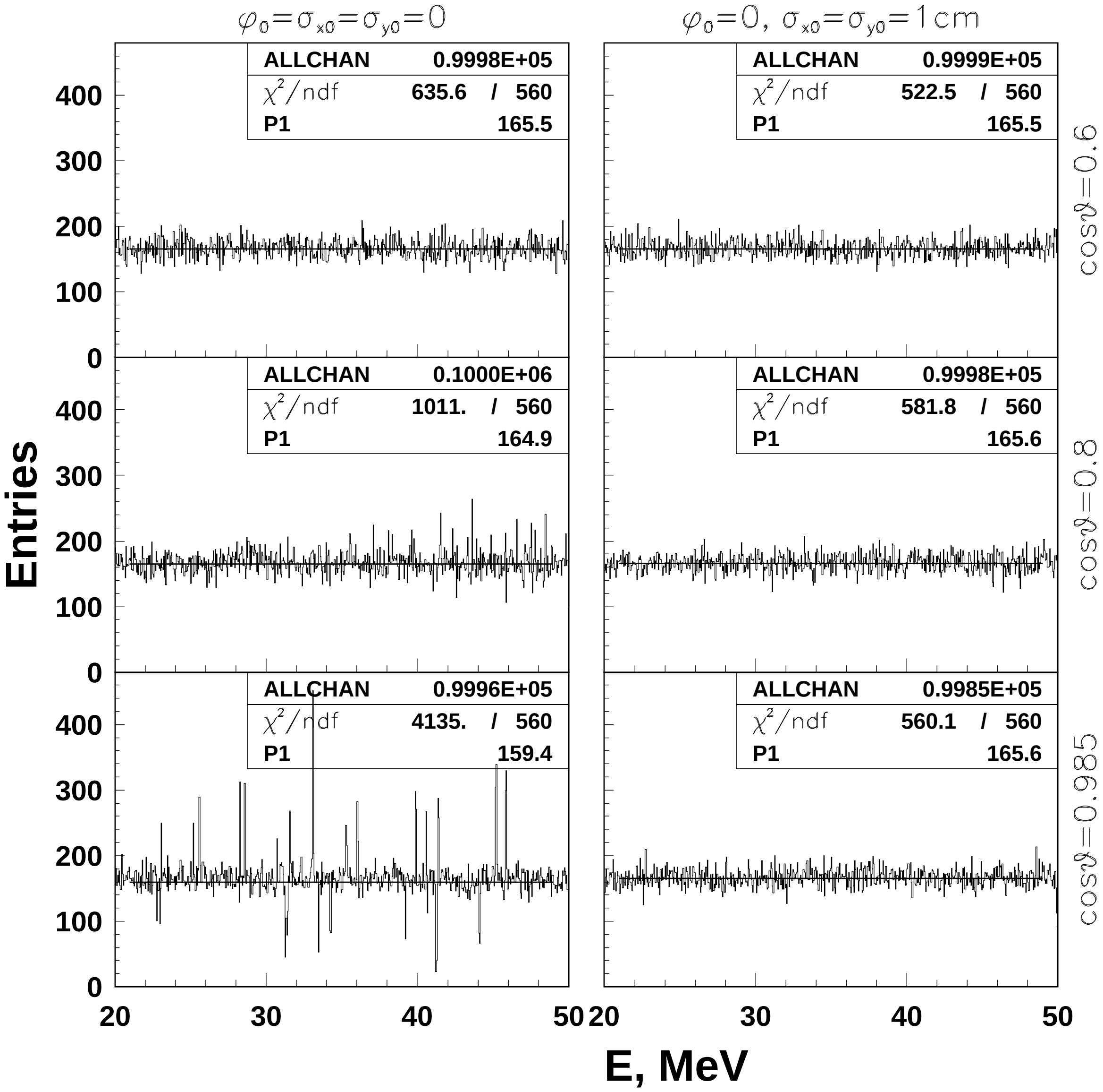

Fig. 16. Fitted energy distribution and its fit to a constant (initial energy distribution was uniform). $\theta_{L,max} = 9^\circ$